How to cite: *Angew. Chem. Int. Ed.* **2020**, *59*, 15191–15194
International Edition: doi.org/10.1002/anie.202005568
German Edition: doi.org/10.1002/ange.202005568

Perovskites

Lead-Free Halide Double Perovskite $Cs_2AgBiBr_6$ with Decreased Band Gap

Fuxiang Ji, Johan Klarbring, Feng Wang, Weihua Ning, Linqin Wang, Chunyang Yin, José Silvestre Mendoza Figueroa, Christian Kolle Christensen, Martin Etter, Thomas Ederth, Licheng Sun, Sergei I. Simak, Igor A. Abrikosov, and Feng Gao**

Abstract: *Environmentally friendly halide double perovskites with improved stability are regarded as a promising alternative to lead halide perovskites. The benchmark double perovskite, $Cs_2AgBiBr_6$, shows attractive optical and electronic features, making it promising for high-efficiency optoelectronic devices. However, the large band gap limits its further applications, especially for photovoltaics. Herein, we develop a novel crystal-engineering strategy to significantly decrease the band gap by approximately 0.26 eV, reaching the smallest reported band gap of 1.72 eV for $Cs_2AgBiBr_6$ under ambient conditions. The band-gap narrowing is confirmed by both absorption and photoluminescence measurements. Our first-principles calculations indicate that enhanced Ag–Bi disorder has a large impact on the band structure and decreases the band gap, providing a possible explanation of the observed band-gap narrowing effect. This work provides new insights for achieving lead-free double perovskites with suitable band gaps for optoelectronic applications.*

Lead (Pb) halide perovskites have attracted intensive attention because of their excellent optoelectronic properties, such as suitable band gaps, long hole-electron diffusion length, and high defect tolerance.[1–4] However, the toxicity of Pb and poor stability represent the main bottlenecks for further commercial applications of these emerging materials. A wide range of different strategies have been employed to develop suitable Pb-free alternatives.[5–9] Among others, one of the most promising approaches is to replace the toxic divalent Pb^{2+} cation with a combination of monovalent and trivalent cations, forming double perovskites.[10–13] Lead-free double perovskites (e.g. $Cs_2AgBiBr_6$) show attractive optical and electronic features.[13,14] However, the large band gap in $Cs_2AgBiBr_6$ is a main reason limiting their photovoltaic performance. To improve their device performance, finding effective strategies to narrow the band gap of the benchmark lead-free double perovskite $Cs_2AgBiBr_6$ is highly desirable.

Along this direction, there have been several structural modification attempts, aiming to decrease the band gap of $Cs_2AgBiBr_6$. For example, Sb impurity doping has been successfully utilized to decrease the band gaps from 2.12 eV to 1.86 eV. The band gap reduction is due to the higher energy levels of Sb 5s states than those of Bi 6s states, raising the valence band maximum slightly.[15] In addition, the phase transition induced by high pressure (15 GPa) leads to the band gap narrowing from original 2.19 eV to 1.70 eV in $Cs_2AgBiBr_6$ crystals.[16] Very recently, a temperature-induced structural change was demonstrated in both $Cs_2AgBiBr_6$ crystals and thin films, resulting in band gap decrease behavior (thermochromism) at high temperatures.[14] Unfortunately, these "low-band gap" phases in the previous reports either still have significantly too large band gaps or are unstable at ambient conditions, limiting their device applications.

Herein, we employ a crystal engineering strategy to modify the benchmark double perovskites $Cs_2AgBiBr_6$. Through simply controlling the crystal growth temperature and growth speed, we obtain modified $Cs_2AgBiBr_6$ crystals with a decreased band gap of 1.72 eV, which is the lowest value among all the reports for pure $Cs_2AgBiBr_6$ at ambient conditions. A 0.26 eV band gap narrowing is confirmed by comparing the absorption and emission spectra between modified and benchmark $Cs_2AgBiBr_6$ crystals. We use density

[*] F. Ji, J. Klarbring, Dr. F. Wang, Dr. W. Ning, Dr. C. Yin, Dr. J. S. M. Figueroa, Prof. T. Ederth, Prof. S. I. Simak, Prof. I. A. Abrikosov, Prof. F. Gao
Department of Physics, Chemistry, and Biology (IFM)
Linköping University
58183 Linköping (Sweden)
E-mail: weihua.ning@liu.se
feng.gao@liu.se
Dr. L. Wang, Prof. L. Sun
Department of Chemistry, KTH Royal Institute of Technology
10044 Stockholm (Sweden)
Dr. C. K. Christensen, Dr. M. Etter
Deutsches Elektronen-Synchrotron (DESY)
22607 Hamburg (Germany)
Prof. L. Sun
State Key Laboratory of Fine Chemicals, Institute of Artificial Photosynthesis, DUT-KTH Joint Education and Research Centre on Molecular Devices, Dalian University of Technology
116024 Dalian (China)
Prof. I. A. Abrikosov
Materials Modeling and Development Laboratory, National University of Science and Technology "MISIS"
Leninskii pr 4, 119049 Moscow (Russia)
Supporting information and the ORCID identification number(s) for the author(s) of this article can be found under: https://doi.org/10.1002/anie.202005568.

functional theory (DFT) calculations to show that the presence of Ag–Bi disorder in $Cs_2AgBiBr_6$ introduces defect states in the gap and, as the disorder level increases, produces a band of defect states.

$Cs_2AgBiBr_6$ single crystals with different band gaps are synthesized by slow evaporation of the precursor solution at different temperatures. The key point to this method is to properly control the growth temperature and growth rate. Figure 1 a is a schematic illustration of the $Cs_2AgBiBr_6$ single crystal preparation. We optimize the growth conditions systematically, and achieve high-quality $Cs_2AgBiBr_6$ crystals at evaporation temperatures of 60 °C (DP-60) and 150 °C (DP-150), respectively. Figure 1 b shows the optical images of DP-60 and DP-150, both of which crystalize in the octahedral shape. As the growth temperature increases from 60 °C to 150 °C, the colors of the resulting $Cs_2AgBiBr_6$ single crystals change from red to black, indicating a wider absorption range. In order to exclude the influence of surface effects, we crush a large black crystal into small pieces, and find that the cross-sections of the small pieces are also black (Figure S1 in the Supporting Information). In addition, by extending the crystal growth time, we achieve a near centimeter-sized single crystal (Figure S2), which is beneficial for single-crystal devices.

We perform X-ray diffraction (XRD) measurements, and exclude the possibility that the color change from DP-60 to DP-150 results from different crystal structures. Single crystal XRD (SCXRD) measurements (Table S1) indicate that both crystals show the typical double-perovskite structure with alternating $AgBr_6$ and $BiBr_6$ octahedra (Figure 1 b). In the DP-150 sample, we observe slight lattice shrink from 11.2695 Å to 11.2636 Å (Table S1), which is also consistent with the powder XRD (PXRD) measurements. The PXRD patterns of DP-60 and DP-150 are nearly identical, matching well with the simulated pattern (Figure 1 c), except for the (400) reflection which shifts slightly toward higher angle for DP-150 (Figure 1 d), confirming slight lattice shrink. These XRD results are also consistent with energy dispersive spectroscopy (EDS) measurements, which indicate that both crystals have similar element distributions (Figure S3).

We quantify the absorption edges of DP-60 and DP-150 by measuring the UV/Vis diffuse reflectance spectra (Figure S4). The reflectance spectra are converted to pseudo-absorbance spectra using the Kubelka-Munk transform.[17] As shown in Figure 2 a, the DP-60 crystal shows a sharp absorption edge at approximately 625 nm, whereas the DP-150 crystal shows an approximately 90 nm red-shift with the absorption edge at around 715 nm. The corresponding band gap calculated from the Tauc plots is reduced from 1.98 eV for DP-60 to 1.72 eV for DP-150 (Figure 2 b), corresponding well with the color change of crystals (Figure 1 b).

We then measure the photoluminescence (PL) spectra of both crystals, and find two interesting observations. Firstly, as shown in Figure 2 c, the PL spectrum of DP-150 shows an obvious red shift compared with that of DP-60. Such a red shift in the PL spectra is consistent with the red shift observed in the absorption measurements, confirming that the absorption edge shift results from the band gap narrowing effect (rather than simply the emergence of isolated defect states without changes to the bands).[18] Secondly, the PL spectra of both crystals are relatively broad, and both of them can be fitted with two Gaussian peaks (Figure S5). A broad PL spectrum in $Cs_2AgBiBr_6$ crystals is consistent with previous reports,[9,15,19] and two Gaussian peaks are ascribed to the emission from the band edge and defect states, respectively.[15] To further understand the defect states, we perform the time-resolved PL for DP-60 and DP-150 single crystals at room temperature, both of which exhibit a fast initial drop followed

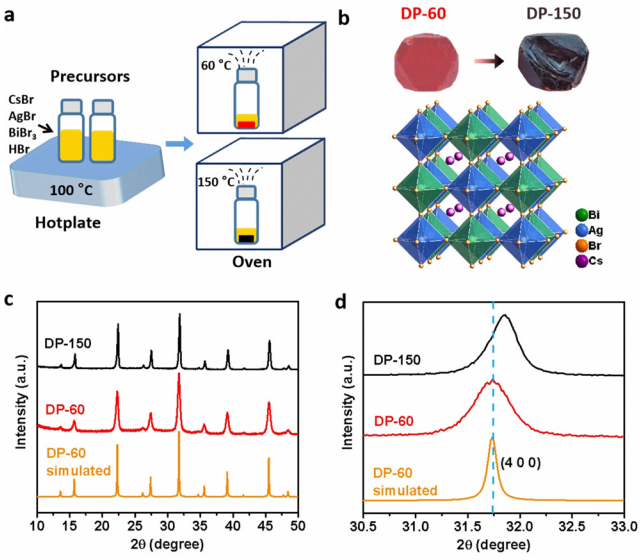

Figure 1. a) Procedure for the crystal growth of DP-60 and DP-150. b) Optical images and the crystal structure of the DP-60 and DP-150 single crystals. c) Normalized PXRD patterns of DP-60 and DP-150 crystals. d) The enlarged view of reflection (400) in the PXRD patterns. The simulated XRD of DP-60 is obtained from Mercury software simulation.

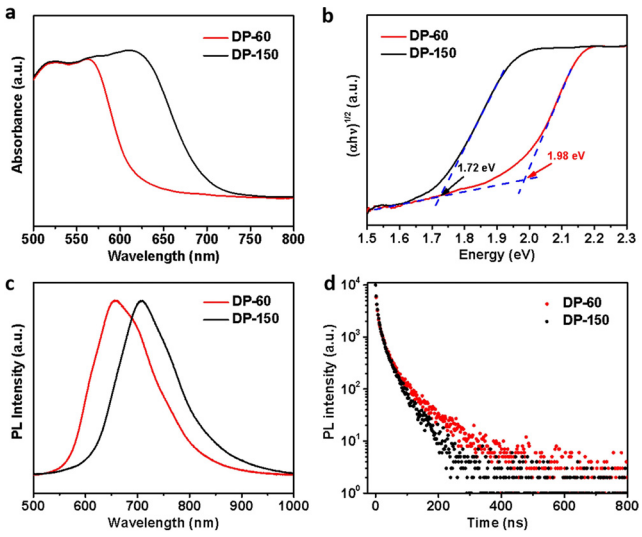

Figure 2. a) Normalized UV/Vis absorption spectra of DP-60 and DP-150 single crystals. b) Tauc plots of DP-60 and DP-150 for indirect band gap semiconductor,[9] showing indirect band gaps of 1.98 eV for DP-60 and 1.72 eV for DP-150. Normalized PL spectra (c) and time-resolved PL (d) of DP-60 and DP-150 single crystals at room temperature.

by a slower decay (Figure 2d). The shorter PL decay time of DP-150, combined with qualitatively weaker PL intensity (Figure S6), indicates more defect states in DP-150.

We are now motivated to understand the origins of defect states and band gap narrowing in our crystals. We are tempted to consider the degree of Ag–Bi disorder as an important source of defect states and band gap narrowing, as different evaporation temperature, which is the only difference when preparing these two different crystals, makes it possible to arrange Ag–Bi atoms in different ways. We note that it is highly challenging to explicitly examine the Ag–Bi disorder in the crystal structure by present characterization techniques (Figure S7). On the other hand, density functional theory (DFT) is known as a reliable tool for investigations of materials properties. We therefore employ first-principles DFT calculations to understand the effect of Ag-Bi disorder on the electronic structure of $Cs_2AgBiBr_6$. We construct supercells with varying degrees of Ag–Bi disorder, ranging from the ideal rocksalt atomic arrangement to a structure representing the completely random 50%–50% alloy on the Ag-Bi sites (see Methods for details). These structures are labeled by a pair of numbers corresponding to the average numbers of nearest neighbors (NNs) of the opposite and the same kind. For example, the perfect rocksalt Ag–Bi ordering is denoted (6,0) since each Ag (Bi) ion has 6 Bi (Ag) and 0 Ag (Bi) NNs. The completely disordered case is hence labelled (3,3).

The (partial) electronic density of states (DOS) of this series of structures, obtained with the hybrid HSE06 functional including spin-orbit coupling (HSE06 + SOC), is shown in Figure 3. In $Cs_2AgBiBr_6$ the top of the valence band is made up primarily of hybridized Ag-d/Br-p states (with some Bi-s character mixed in at the band edge), while the conduction band is made up of Bi-p/Br-p states. The (5.5,0.5) structure corresponds to one NN Ag-Bi antisite pair in the supercell, that is, in the otherwise perfect rocksalt structure the positions of one Ag and one Bi are swapped. We see that this introduces an acceptor-like defect state of Bi-p/Br-p character into the band gap. This type of defect state could be responsible for the double-peak nature of the PL emission of DP-60, discussed above. As the disorder is further increased, this defect state moves deeper into the gap and another, progressively broader set of defect states are formed below the conduction band edge. In addition, an occupied defect state of Ag-d/Br-p character emerges from the valence band edge into the gap (at $E = 0$ in the (4.5,1.5) structure). Figure S8 displays effective band structures obtained with the PBEsol functional for the (5.5,0.5) and the (4.5,1.5) structures.

A quantitative statement regarding the actual level of the Ag–Bi disorder in our DP-60 and DP-150 crystals cannot be made with available data. However, the qualitative picture of a set of defect states that progressively emerges from the conduction band edge, and broadens, as the Ag–Bi disorder is increased (Figure 3), is consistent with the observed red-shift of the absorption edge of DP-150 in comparison to the DP-60 being an effect of an increase in Ag–Bi disorder, and with the dual-peak nature of the PL spectra of both crystals.

In addition, stability is an important issue to evaluate with regards to the potential use of perovskite materials for optoelectronic applications. We have therefore investigated the environmental stability of the DP-150 $Cs_2AgBiBr_6$ double perovskites. The PXRD measurements (Figure 4a) indicate that the freshly prepared DP-150 crystals show no signs of decomposition for up to 240 days in the ambient atmosphere. In addition, this excellent stability of DP-150 is also confirmed by complementary characterization techniques (Raman, absorption and PL spectra). The Raman band located at 178 cm^{-1} belongs to the symmetric stretching of Br atoms around Bi atoms in the octahedron,[20] showing that no changes in the molecular bonds of the crystalline structure are

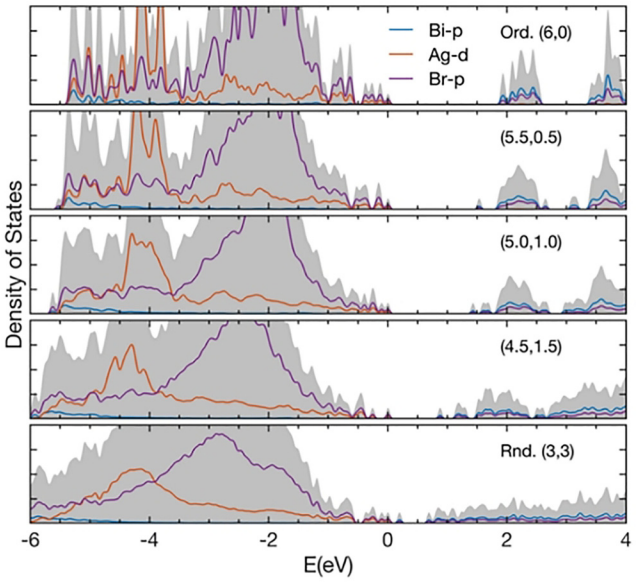

Figure 3. Calculated total and partial electronic density of states for a set of $Cs_2AgBiBr_6$ structures with varying degrees of Ag–Bi disorder (see text). The energy, *E*, is set to zero at the highest occupied state for each separate structure.

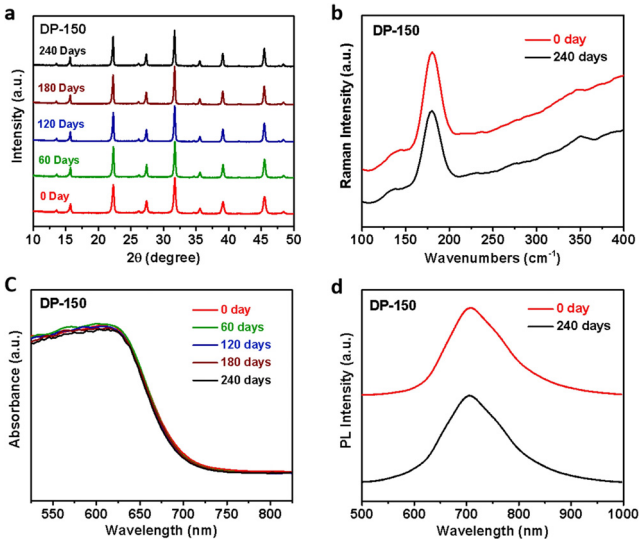

Figure 4. Time-dependent PXRD (a), Raman spectra (b), UV/Vis absorption spectra (c) and PL spectra (d) of DP-150 after exposure to ambient conditions.

present after a long time (Figure 4b). Figure 4c,d show the absorption and PL spectra of DP-150, where negligible changes are observed after exposure to ambient atmosphere for 240 days, demonstrating excellent stability of DP-150. Such a superior environmental stability makes DP-150 a promising candidate for applications in highly stable single crystal optoelectronic devices.

In summary, we achieve the smallest reported band gap lead-free double perovskite $Cs_2AgBiBr_6$ through controlling the growth temperature of single crystals. Although different growth temperatures have no effect on the crystal structures, the crystal prepared from high evaporation temperature (DP-150) shows a significant band gap narrowing (ca. 0.26 eV) compared with that prepared from the low evaporation temperature (DP-60). We hypothesize that this band gap narrowing is caused by an increased level of Ag–Bi disorder in DP-150 as compared to DP-60. First-principles calculations show that when such disorder is introduced and progressively increased, it initially results in isolated defect states in the gap and eventually produces a band of defect states. We believe that the DP-150 single crystals with decreased band gap could be suitable for high-efficiency and stable single crystal devices, such as solar cells and photodetectors. In addition, our results provide a simple yet effective way to optimize the band gap of double perovskites and may be applicable to other crystalline materials as well.

Acknowledgements

We thank Prof. L. Zhang (Jilin University) and Prof. J. Birch (Linköping University) for helpful discussions. This work was financially supported by Knut and Alice Wallenberg Foundation, the Swedish Energy Agency (2018-004357), VR Starting Grant (2019-05279), Carl Tryggers Stiftelse, Olle Engkvist Byggmästare Stiftelse, and the Swedish Government Strategic Research Area in Materials Science on Functional Materials at Linköping University (Faculty Grant SFO-Mat-LiU No. 2009-00971). L.S. would like to thank the Swedish Energy Agency, and SSF for financial support. L.W. acknowledges the Diamond Light Source for access to beamline I19 (MT20805), and thanks Dr. L. Saunders and Dr. D. Allan for technical support. F.J. and L.W. were supported by the China Scholarship Council (CSC). F.W. is a Marie Skłodowska-Curie Fellow (No. 751375). F.G. is a Wallenberg Academy Fellow. I.A.A. is a Wallenberg Scholar. Theoretical analysis of calculated properties was supported by the Ministry of Science and High Education of the Russian Federation in the framework of MegaGrant (no. 075-15-2019-872 (14.Y26.31.0027/074-02-2018-327)). The support from Swedish Research Council (VR) (Project No. 2019-05551) is acknowledged by S.I.S. and J.K. The computations were enabled by resources provided by the Swedish National Infrastructure for Computing (SNIC) at the PDC Centre for High Performance Computing (PDC-HPC) and the National Supercomputer Center (NSC) partially funded by the Swedish Research Council through grant agreement no. 2016-07213.

Conflict of interest

The authors declare no conflict of interest.

Keywords: Ag–Bi disorder · band-gap engineering · crystal engineering · $Cs_2AgBiBr_6$ · lead-free double perovskites

[1] A. Kojima, K. Teshima, Y. Shirai, T. Miyasaka, *J. Am. Chem. Soc.* **2009**, *131*, 6050 – 6051.
[2] N. J. Jeon, J. H. Noh, W. S. Yang, Y. C. Kim, S. Ryu, J. Seo, S. I. Seok, *Nature* **2015**, *517*, 476 – 480.
[3] S. D. Stranks, G. E. Eperon, G. Grancini, C. Menelaou, M. J. P. Alcocer, T. Leijtens, L. M. Herz, A. Petrozza, H. J. Snaith, *Science* **2013**, *342*, 341 – 344.
[4] C. Ran, J. Xu, W. Gao, C. Huang, S. Dou, *Chem. Soc. Rev.* **2018**, *47*, 4581 – 4610.
[5] W. Ning, F. Gao, *Adv. Mater.* **2019**, *31*, 1900326.
[6] F. Hao, C. C. Stoumpos, D. H. Cao, R. P. H. Chang, M. G. Kanatzidis, *Nat. Photonics* **2014**, *8*, 489 – 494.
[7] B.-W. Park, B. Philippe, X. Zhang, H. Rensmo, G. Boschloo, E. M. J. Johansson, *Adv. Mater.* **2015**, *27*, 6806 – 6813.
[8] M. Chen, M.-G. Ju, A. D. Carl, Y. Zong, R. L. Grimm, J. Gu, X. C. Zeng, Y. Zhou, N. P. Padture, *Joule* **2018**, *2*, 558 – 570.
[9] A. H. Slavney, T. Hu, A. M. Lindenberg, H. I. Karunadasa, *J. Am. Chem. Soc.* **2016**, *138*, 2138 – 2141.
[10] X.-G. Zhao, J.-H. Yang, Y. Fu, D. Yang, Q. Xu, L. Yu, S.-H. Wei, L. Zhang, *J. Am. Chem. Soc.* **2017**, *139*, 2630 – 2638.
[11] W. Pan, H. Wu, J. Luo, Z. Deng, C. Ge, C. Chen, X. Jiang, W.-J. Yin, G. Niu, L. Zhu, et al., *Nat. Photonics* **2017**, *11*, 726 – 732.
[12] J. Luo, X. Wang, S. Li, J. Liu, Y. Guo, G. Niu, L. Yao, Y. Fu, L. Gao, Q. Dong, et al., *Nature* **2018**, *563*, 541 – 545.
[13] W. Ning, F. Wang, B. Wu, J. Lu, Z. Yan, X. Liu, Y. Tao, J.-M. Liu, W. Huang, M. Fahlman, et al., *Adv. Mater.* **2018**, *30*, 1706246.
[14] W. Ning, X.-G. Zhao, J. Klarbring, S. Bai, F. Ji, F. Wang, S. I. Simak, Y. Tao, X.-M. Ren, L. Zhang, et al., *Adv. Funct. Mater.* **2019**, *29*, 1807375.
[15] K. Du, W. Meng, X. Wang, Y. Yan, D. B. Mitzi, *Angew. Chem. Int. Ed.* **2017**, *56*, 8158 – 8162; *Angew. Chem.* **2017**, *129*, 8270 – 8274.
[16] Q. Li, Y. Wang, W. Pan, W. Yang, B. Zou, J. Tang, Z. Quan, *Angew. Chem. Int. Ed.* **2017**, *56*, 15969 – 15973; *Angew. Chem.* **2017**, *129*, 16185 – 16189.
[17] P. Kubelka, F. Munk, *Z. Tech. Phys.* **1931**, *12*, 16.
[18] P. K. Nayak, M. Sendner, B. Wenger, Z. Wang, K. Sharma, A. J. Ramadan, R. Lovrinčić, A. Pucci, P. K. Madhu, H. J. Snaith, *J. Am. Chem. Soc.* **2018**, *140*, 574 – 577.
[19] L. Schade, A. D. Wright, R. D. Johnson, M. Dollmann, B. Wenger, P. K. Nayak, D. Prabhakaran, L. M. Herz, R. Nicholas, H. J. Snaith, et al., *ACS Energy Lett.* **2019**, *4*, 299 – 305.
[20] S. J. Zelewski, J. M. Urban, A. Surrente, D. K. Maude, A. Kuc, L. Schade, R. D. Johnson, M. Dollmann, P. K. Nayak, H. J. Snaith, et al., *J. Mater. Chem. C* **2019**, *7*, 8350 – 8356.

Manuscript received: April 16, 2020
Accepted manuscript online: May 15, 2020
Version of record online: June 22, 2020

